Multichannel ballistic magnetotransport through quantum wires with double circular bends

Karel Vacek, Ayao Okiji, and Hideaki Kasai
Department of Applied Physics, Osaka University, Suita, Osaka 565, Japan
(Received 8 September 1992)

A theoretical study of magnetotransport through two-dimensional quantum wires with double circular bends is made within the ballistic approximation. By means of the mode-matching method, the S matrix of the single bend with a hard-wall confining potential is calculated as a function of the magnetic field or the Fermi energy for the bending radius and the bending angle as parameters. The combination of S matrices is performed for bends in series. The technique is applied to systems consisting of double bends. The symmetry properties of the S matrix are clarified for the two-terminal systems with rotational symmetry or mirror-plane symmetry. The transmission matrix is evaluated in detail for the case of three propagating channels. The strong dependence of the interchannel scattering on the magnetic field is found. The structure of dips (antiresonances) appearing in the conductance is studied as a function of the distance between bends.

I. INTRODUCTION

During the past decade, there has been a rapid development in the physics of semiconductor nanostructures.[1] Experimentally, many interesting effects have been observed in the magnetotransport of quantum wires, e.g., the anomalous quenching of the quantum Hall effect,[2–4] the negative bend resistance,[5] and the energy gaps and minibands in the periodic stub structure.[6] The models of these quantum-wire systems are usually solved numerically by the coupled-channel method,[7–10] by the mode-matching method,[11–13] or by the recursive calculation of the discrete Green function.[14,15]

There are groups of studies on the ballistic transport and bound states in open systems like the cross-shaped junction[16–19] and the broken-strip configuration with a right angle[19–23] or with an arbitrary angle.[24,25] The broken-strip configurations are studied mainly in the absence of magnetic fields. The external magnetic fields have been considered only by Schult, Wyld, and Ravenhall.[19] The resonance effects have been found experimentally[26] in the broken-strip double bend with right angles. As for the single circular bends, there are studies concerned with bound states[23,27–29] and transmission probabilities[29–31] in the absence of magnetic fields. In a previous Letter[32] and paper,[33] we have included external magnetic fields in the treatment of single circular bends.

Being motivated by the recent measurement[34] of the entire transmission matrix of the mesoscopic conductor, we want to present a study of simple quantum devices in which the conductance plateaus are almost unchanged over a wide range of parameters. However, the intermode scattering is strong and depends on the applied magnetic field. The devices are tentatively proposed to be built from double circular bendings of an otherwise uniform two-dimensional quantum wire. We also investigate the sharp increase of the backward scattering in the limited regions of Fermi energies where narrow dips appear in conductance plateaus. The paper is organized as follows. In Sec. II, we consider quantum motion of a charged particle in circular bends with a hard-wall confining potential in the presence of magnetic fields. Then we determine the S matrix and perform the combination of S matrices in order to calculate the transport properties of bends in series. In Sec. III, we study the system of double circular bends separated by a piece of the straight wire of various lengths. In Sec. IV, the conclusion is given and some of the yet open questions are stated. In the Appendix, the properties of wave functions in bent quantum wires in the presence of magnetic fields are discussed.

II. THE MODEL

Due to symmetry, there are two different possibilities of how to combine two bends. One arrangement is with bends turning to alternative directions. We choose bends turning to the left and to the right, called an S-shaped system, as shown schematically in Fig. 1(a). Another combination is with both bends turning to the same direction. The system with both bends turning to the

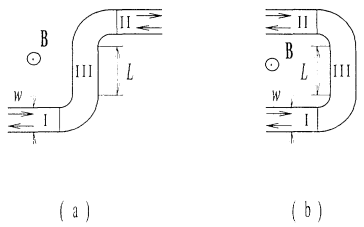

FIG. 1. The schematic view of quantum wires with double circular bends: (a) the S-shaped system (represented by a combination of the left-turned and right-turned bends), (b) the U-shaped system (represented by a combination of two left-turned bends). The width of the wires is w and the distance between bends is L. The potential is zero inside wires, and infinite outside. The magnetic field **B** points out from the picture. The bending angle of individual bends is not required to be equal to $\pi/2$.

left, called a U-shaped system, is shown in Fig. 1(b). Since we limit ourselves to the ballistic approximation, the transport properties of these systems are determined by the scattering matrix (the S matrix).

A. The S matrix

The Hamiltonian for ballistic motion of a single electron of effective mass m^* and charge $-e$ in the two-dimensional quantum wire is

$$H=\frac{1}{2m^*}\left[-i\hbar\nabla+\frac{e}{c}\mathbf{A}\right]^2+V\ , \tag{2.1}$$

where V is the confinement potential and $\mathbf{A}$ is the vector potential of the external magnetic field $\mathbf{B}=(0,0,B)$. Let us consider multichannel transport through the scattering region in the quantum wire (see Fig. 1). The Schrödinger equation in a perfect lead of width w (region I) stretching from the scattering region III can be written as

$$\left\{\frac{\hbar^2}{2m^*}\left[\left[\frac{\partial}{\partial x_1}-i\frac{eB}{\hbar c}y_1\right]^2+\frac{\partial^2}{\partial y_1^2}\right]+E_F-V(x_1,y_1)\right\}\Psi^{(\mathrm{I})}(x_1,y_1)=0\ , \tag{2.2}$$

where we use the Landau gauge, $\mathbf{A}^{(\mathrm{I})}=(-y_1B,0,0)$. The longitudinal x_1 and transverse y_1 variables are separable. The solution is

$$\Psi^{(\mathrm{I})}(x_1,y_1)=\sum_{l=1}^{\infty}f(y_1,p_l)\exp(ip_lx_1)a_l^{(+)}+\sum_{l=1}^{\infty}f(y_1,-p_l)\exp(-ip_lx_1)a_l^{(-)}\ , \tag{2.3}$$

where $a_l^{(\pm)}$ are the mode amplitudes. The wave function $\Psi^{(\mathrm{II})}(x_2,y_2)$ with the mode amplitudes $b_l^{(\pm)}$ in region II is written similarly. We approximate the confinement potential by the hard-wall type, $V(x_i,y_i)=0$ for $-w/2<y_i<w/2$ and $V(x_i,y_i)=\infty$ elsewhere, $i=1$ and 2. The transverse wave functions $f(y,p_l),l=1,2,\ldots,\infty$, then satisfy the equation

$$\left[\frac{d^2}{dy^2}+\frac{\pi^2}{w^2}\epsilon_F-\left[p_l-\frac{\mathcal{B}}{w^2}y\right]^2\right]f(y,p_l)=0\ , \tag{2.4}$$

with the boundary condition $f(y,p_l)=0$ for $y=-w/2,w/2$. For convenience, we use the dimensionless Fermi energy $\epsilon_F=E_F/E_1$, where $E_1=\hbar^2\pi^2/2m^*w^2$ is the energy threshold for propagation in the lowest subband in a perfect wire for zero magnetic field. The dimensionless magnetic field is $\mathcal{B}=B/B_0$, where $B_0=\hbar c/ew^2$. The transverse wave functions possess symmetry $f(y,-p_l,B)=(-1)^{l+1}f(-y,p_l,B)$.

The incoming amplitudes $a^{(+)}$ and $b^{(-)}$ and the outgoing amplitudes $b^{(+)}$ and $a^{(-)}$ are shown schematically in Fig. 2(a). The scattering matrix $[s]$ relates the incoming and the outgoing channels in the following way:

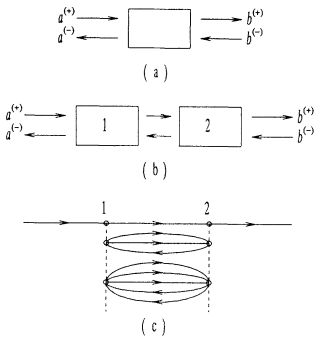

FIG. 2. (a) The schematic picture of a scatterer in the quantum wire. The incoming amplitudes are vectors $a^{(+)}$ and $b^{(-)}$ of the size $M\times1$, the outgoing amplitudes are vectors $a^{(-)}$ and $b^{(+)}$ of the same size. (b) The schematic picture of the combination of two scatterers in series. (c) The diagrammatic representation of the scattering matrix as the result of the combination of two scatterers in the quantum wire. Only the series for the submatrix t is shown; the submatrices r, $\tilde{t}$, and $\tilde{r}$ are obtained similarly.

$$\begin{bmatrix}b^{(+)}\\a^{(-)}\end{bmatrix}=[s]\begin{bmatrix}a^{(+)}\\b^{(-)}\end{bmatrix},\quad [s]=\begin{bmatrix}t & \tilde{r}\\ r & \tilde{t}\end{bmatrix}\ , \tag{2.5}$$

where t and r are the submatrices of the transmission and the reflection amplitudes for an electron incoming from region I. Similarly, $\tilde{t}$ and $\tilde{r}$ are the submatrices of the transmission and the reflection amplitudes for an electron incoming from region II.

B. The combination of S matrices

For the scattering region divided into two regions with S matrices $[s_1]$ and $[s_2]$ [cf. Fig. 2(b)], the total S matrix $[s]$ can be represented as in Fig. 2(c). This leads to formulas

$$t=t_2(I-\tilde{r}_1r_2)^{-1}t_1\ , \tag{2.6a}$$

$$r=r_1+\tilde{t}_1r_2(I-\tilde{r}_1r_2)^{-1}t_1\ , \tag{2.6b}$$

$$\tilde{t}=\tilde{t}_1[I+r_2(I-\tilde{r}_1r_2)^{-1}\tilde{r}_1]\tilde{t}_2\ , \tag{2.6c}$$

$$\tilde{r}=\tilde{r}_2+t_2(I-\tilde{r}_1r_2)^{-1}\tilde{r}_1\tilde{t}_2\ . \tag{2.6d}$$

In the presence of magnetic fields, this sequence of submatrices cannot be reversed. Usually, when we consider multichannel ballistic transport in mesoscopic systems, we use only the asymptotic limit of the scattering matrix, which enables us to calculate the two-terminal conductance G from the Landauer formula,

$$G=\frac{2e^2}{h}\sum_{m,n=1}^{N}t_{mn}^*t_{mn}\ , \tag{2.7}$$

and to monitor the unitarity condition,

$$\sum_{l=1}^{N}t_{lm}^*t_{ln}+\sum_{l=1}^{N}r_{lm}^*r_{ln}=\delta_{mn}\ . \tag{2.8}$$

Here, N denotes the number of propagating channels in perfect leads. However, in the present situation we need

to combine two scatterers which are a *finite* distance apart. Thus we must consider scattering matrices *including the evanescent channels.* In spite of the number of evanescent channels being infinite, we will consider only M propagating and evanescent channels together. The number of channels M is large enough to achieve convergency. After performing the necessary combinations, we will use again only the asymptotic limit of the total scattering matrix to obtain the two-terminal conductance from Eq. (2.7).

C. The S matrices for individual scattering regions

Here, we describe the scattering matrices of left-turned and right-turned bends and of an intermediate piece of the straight wire. The scattering matrix $[s^s]$ for a piece of the straight wire of length L is

$$[s^s]=\begin{bmatrix} t^s & \tilde{r}^s \\ r^s & \tilde{t}^s \end{bmatrix}, \tag{2.9}$$

see Fig. 3(a). The trivial matching at the boundary I-III and III-II gives $t^s_{mn}=\tilde{t}^s_{mn}=\exp(ip_mL)\delta_{mn}, r^s_{mn}=\tilde{r}^s_{mn}=0$. The perfect wire introduces no coupling between channels and no backscattering. The only effect of the straight wire appears in the phase shifts of the diagonal elements in the transmission submatrix.

The scattering matrix $[s^L]$ of the left-turned bend with bending radius R_0 and bending angle Θ [cf. Fig. 3(b)] is

$$[s^L]=\begin{bmatrix} t^L & \tilde{r}^L \\ r^L & \tilde{t}^L \end{bmatrix}. \tag{2.10}$$

The Schrödinger equation in the left-turned bend in polar coordinates can be written as

$$\left\{\frac{\hbar^2}{2m^*}\left[\frac{\partial^2}{\partial r^2}+\frac{1}{r}\frac{\partial}{\partial r}-\left[\frac{eB}{2\hbar c}r-\frac{i}{r}\frac{\partial}{\partial\varphi}\right]^2\right]+E_F-V(r,\varphi)\right\}\Psi^{(\mathrm{III})}(r,\varphi)=0, \tag{2.11}$$

where the symmetric gauge is used, $A^{(\mathrm{III})}_{\varphi}=Br/2$. By separation of variables, $\Psi^{(\mathrm{III})}(r,\varphi)$ can be solved as

$$\Psi^{(\mathrm{III})}(r,\varphi)=\sum_{l=1}^{\infty} g(r,\nu_l^{(+)})\exp(i\nu_l^{(+)}\varphi)c_l^{(+)}+\sum_{l=1}^{\infty} g(r,\nu_l^{(-)})\exp(i\nu_l^{(-)}\varphi)c_l^{(-)}, \tag{2.12}$$

where $c_l^{(\pm)}$ are the mode amplitudes in the bend. The transverse wave function g and the eigenvalues $\nu_l^{(\pm)}$, $l=1,2,\ldots,\infty$, satisfy the eigenvalue equation

$$\left\{\frac{d^2}{dr^2}+\frac{1}{r}\frac{d}{dr}+\frac{\pi^2}{w^2}\epsilon_F-\left[\frac{\nu_l^{(\pm)}}{r}+\frac{\mathcal{B}}{2w^2}r\right]^2\right\}g(r,\nu_l^{(\pm)})=0, \tag{2.13}$$

with the boundary condition $g(r,\nu_l^{(\pm)})=0$ for $r=R_0,R_0+w$. We associate a discrete set of eigenvalues $\nu_l^{(+)}$, $l=1,2,\ldots,\infty$, with the motion of the electron in the positive direction of angle φ. Similarly, we associate a discrete set of eigenvalues $\nu_l^{(-)}$, $l=1,2,\ldots,\infty$, with the motion of the electron in the negative direction of angle φ. The orthogonalization and normalization to the unit flux in each channel in the bend region are shown in the Appendix. For $\mathcal{B}=0$, there is a simple relation of $\nu_l^{(-)}=-\nu_l^{(+)}$. The transverse functions are then the same for the motion in both directions $g(r,\nu_l)=g(r,-\nu_l)$ and can be expressed by Bessel functions of the first and second kind.

In order to unify the gauges into the symmetric type, the wave functions are multiplied by appropriate phase

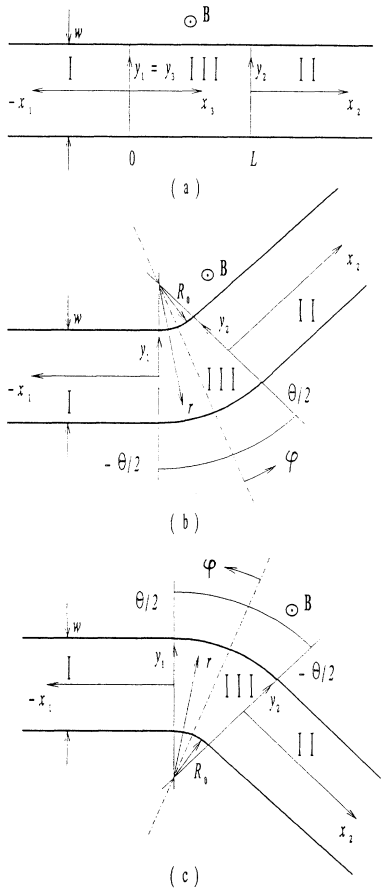

FIG. 3. The geometry of individual scatterers considered in our study. The regions I and II represent perfect leads stretching out to infinity, and the region III represents the scatterer. The local Cartesian coordinates in the left (right) lead are x_1, y_1 (x_2, y_2). The zeros of the x_1 and x_2 coordinates are at the boundaries I-III and III-II, respectively. The zeros of the y_1 and y_2 coordinates are on the axes of the wire in regions I and II, respectively. The width of the wire w is the same in all regions. (a) The trivial case of a scatterer: a piece of the straight wire of length L. (b) The left-turned bend of bending radius R_0 (=inner radius) and of bending angle Θ acting as a scatterer. (c) The right-turned bend of the same parameters as the left-turned bend. The bends possess the mirror-plane symmetry according to the axis of $\varphi=0$ (dash-dotted line).

factors.[32] Next, the continuity of the wave function and of its normal derivative are required. In the matching of the wave function in the left-turned bend, the transverse coordinates y_1, y_2, and r have opposite orientation at the interfaces I-III and III-II, namely, $y_1=-r+R_0+w/2$ at I-III and $y_2=-r+R_0+w/2$ at III-II. By mode matching, we obtain a set of linear equations for the submatrices t^L, r^L and the amplitudes $c^{(+)}$, $c^{(-)}$,

$$\sum_{m=1}^{\infty} f\left[-r+R_0+\frac{w}{2},p_m\right]\delta_{mn}+\sum_{m=1}^{\infty} f\left[-r+R_0+\frac{w}{2},-p_m\right]r^L_{mn}$$
$$=\sum_{l=1}^{\infty} g(r,\nu_l^{(+)})\exp\left[-i\nu_l^{(+)}\frac{\Theta}{2}\right]c_{ln}^{(+)}+\sum_{l=1}^{\infty} g(r,\nu_l^{(-)})\exp\left[-i\nu_l^{(-)}\frac{\Theta}{2}\right]c_{ln}^{(-)}\ , \tag{2.14a}$$

$$\sum_{m=1}^{\infty} f\left[-r+R_0+\frac{w}{2},p_m\right]\left[-\frac{i\mathcal{B}}{2w^2}(2R_0+w-r)+ip_m\right]\delta_{mn}$$
$$+\sum_{m=1}^{\infty} f\left[-r+R_0+\frac{w}{2},-p_m\right]\left[-\frac{i\mathcal{B}}{2w^2}(2R_0+w-r)-ip_m\right]r^L_{mn}$$
$$=\frac{1}{r}\sum_{l=1}^{\infty} g(r,\nu_l^{(+)})i\nu_l^{(+)}\exp\left[-i\nu_l^{(+)}\frac{\Theta}{2}\right]c_{ln}^{(+)}+\frac{1}{r}\sum_{l=1}^{\infty} g(r,\nu_l^{(-)})i\nu_l^{(-)}\exp\left[-i\nu_l^{(-)}\frac{\Theta}{2}\right]c_{ln}^{(-)}\ , \tag{2.14b}$$

$$\sum_{m=1}^{\infty} f\left[-r+R_0+\frac{w}{2},p_m\right]t^L_{mn}=\sum_{l=1}^{\infty} g(r,\nu_l^{(+)})\exp\left[i\nu_l^{(+)}\frac{\Theta}{2}\right]c_{ln}^{(+)}+\sum_{l=1}^{\infty} g(r,\nu_l^{(-)})\exp\left[i\nu_l^{(-)}\frac{\Theta}{2}\right]c_{ln}^{(-)}\ , \tag{2.14c}$$

$$\sum_{m=1}^{\infty} f\left[-r+R_0+\frac{w}{2},p_m\right]\left[-\frac{i\mathcal{B}}{2w^2}(2R_0+w-r)+ip_m\right]t^L_{mn}$$
$$=\frac{1}{r}\sum_{l=1}^{\infty} g(r,\nu_l^{(+)})i\nu_l^{(+)}\exp\left[i\nu_l^{(+)}\frac{\Theta}{2}\right]c_{ln}^{(+)}+\frac{1}{r}\sum_{l=1}^{\infty} g(r,\nu_l^{(-)})i\nu_l^{(-)}\exp\left[i\nu_l^{(-)}\frac{\Theta}{2}\right]c_{ln}^{(-)}\ . \tag{2.14d}$$

Equations (2.14a) and (2.14b) match the wave function and its normal derivative, respectively, at the interface I-III. Similarly, Eqs. (2.14c) and (2.14d) match the wave function and its normal derivative at the interface II-III. To solve Eqs. (2.14a)–(2.14d) numerically, we use a discrete fine mesh instead of the continuous variable r and calculate the submatrices t^L and r^L in detail. Since the determination of t^L and r^L requires substantial computational effort, it is desirable to obtain submatrices $\tilde{t}^L$ and $\tilde{r}^L$ from t^L and r^L by means of the symmetry relations. Writing the matching equations for the submatrices $\tilde{t}^L$ and $\tilde{r}^L$ and inverting the magnetic field, $B\rightarrow -B$, in Eqs. (2.14a)–(2.14d) yield the relations

$$\tilde{t}^L_{mn}(B)=t^L_{mn}(-B)\ , \tag{2.15a}$$

$$\tilde{r}^L_{mn}(B)=r^L_{mn}(-B)\ . \tag{2.15b}$$

Equations (2.15a) and (2.15b) are not obtained from the multichannel reciprocity theorem[35] for the scattering matrix. Rather, they are related to Eqs. (2.14a)–(2.14d) by the mirror-plane symmetry of the bend according to the axis shown in Fig. 3(b). The reciprocity theorem, which requires the transposition of the submatrix t, represents an independent relation that holds in any system regardless of its geometrical symmetry. We will use the reciprocity theorem in Sec. III together with the geometrical symmetry relations to show the symmetry properties of the S matrix for various systems.

The last element of which we must find the S matrix is the right-turned bend, cf. Fig. 3(c),

$$[s^R]=\begin{bmatrix} t^R & \tilde{r}^R \\ r^R & \tilde{t}^R \end{bmatrix}\ . \tag{2.16}$$

The treatment of the bend region is the same as for the left-turned bend. The difference comes in the gauge phase factors and in the matching equations. Furthermore, the transverse coordinates y_1, y_2, and r are in the same direction at the interfaces I-III and III-II, respectively ($y_1=r-R_0-w/2$ at I-III and $y_2=r-R_0-w/2$ at III-II). Writing the matching equations for the submatrices t^R, r^R and using the symmetry properties of functions $f(y,p_l)$ in Eqs. (2.14a)–(2.14d) yield the relations

$$t^R_{mn}(B)=(-1)^{m+n}\tilde{t}^L_{mn}(B)\ , \tag{2.17a}$$

$$r^R_{mn}(B)=(-1)^{m+n}\tilde{r}^L_{mn}(B)\ . \tag{2.17b}$$

The submatrices $\tilde{t}^R, \tilde{r}^R$ are obtained from relations similar to Eqs. (2.15a) and (2.15b).

A single-channel model was used in Ref. 23 for the S-shaped and U-shaped broken-strip double bend with right angles. In the single-channel approximation, there is no difference between the S matrices $[s^L]$ and $[s^R]$ in the absence of magnetic fields [see Eqs. (2.15) and (2.17)]. However, there is a difference between right-turned and left-turned bends in general. This difference appears when one considers two or more channels.

III. RESULTS AND DISCUSSION

Transport in the lowest three subbands ($1 \leq l \leq 3$) is investigated. The effective mass of an electron (in GaAs) $m^* \simeq 0.067 m_e$ (m_e is the free-electron mass) and the width of quantum wires $w \simeq 75$ nm according to previous experimental works[1] are assumed. The unit of energy is then $E_1 \simeq 1.0$ meV and the unit of the magnetic field is $B_0 \simeq 0.12$ T. A bending radius $R_0 = 0.5w$ or $R_0 = 0.25w$, and bending angle $\Theta = \pi/2$ are considered. A magnetic field of $|B| \leq 26B_0$ is used.

The method appears to be numerically very stable with fast convergency. The channel expansion is done usually up to eight channels and the results are obtained mainly within five-digit accuracy. Equation (2.6) can become unstable for $I - \tilde{r}_1 r_2$ close to the singular matrix, i.e., for the strong backscattering. The strong backscattering is only around the conductance dips, which are limited to the narrow regions of the effectively negative potential, as we have shown earlier.[32] Even in the vicinity of the conductance dips, the unitarity is preserved very well, at least to three digits.

An example of the transverse eigenfunctions in the bent quantum wire is shown below. The seven lowest modes $g(r, \nu_l^{(\pm)})$ in the left-turned and right-turned bends for $R_0 = 0.25w$, $E_F = 10.0E_1$, and $B = 10.0B_0$ are plotted in Fig. 4. The propagating modes, in this case $l = 1$, 2, and 3, are real and they split according to the motion in the positive (+) or the negative (−) direction of angle φ [cf. Fig. 4(a)]. As for the evanescent modes, here $l = 4$, 5, 6, and 7, only the modes corresponding to the penetration of an electron in the positive direction of angle φ are shown in Figs. 4(b) and 4(c). The evanescent modes corresponding to the penetration in the negative direction of angle φ are the complex conjugate of the plotted functions.

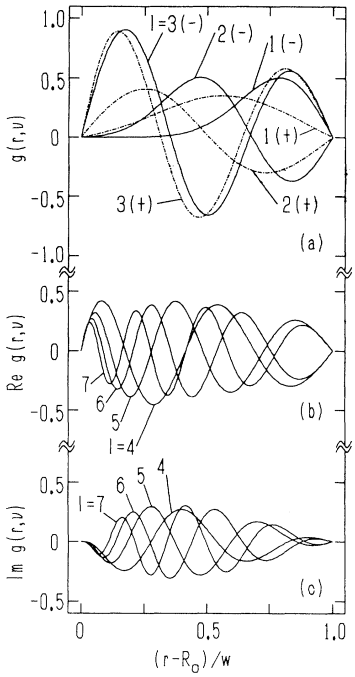

FIG. 4. The shape of the transverse eigenfunctions $g(r, \nu_l^{(\pm)})$ in the left-turned and right-turned bends for $R_0 = 0.25w$, $E_F = 10E_1$, and $B = 10B_0$. (a) The propagating modes $l = 1$, 2, and 3, corresponding to the motion of an electron in the positive direction of angle φ (dash-dotted curves) and in the negative direction of angle φ (solid curves). (b) The real part of the evanescent modes $l = 4$, 5, 6, and 7. (c) The imaginary part of the evanescent modes $l = 4$, 5, 6, and 7, corresponding to the penetration of an electron in the positive direction of angle φ. The evanescent modes corresponding to the penetration in the negative direction of angle φ can be obtained by complex conjugation of the function g.

A. Matrix of transmission probabilities

The transmission probabilities T_{mn} from the channel n in region I into the channel m in region II are $|t_{mn}|^2$. The dependence of the matrix of the transmission probabilities on the magnetic field for the case of three open channels in the asymptotic regions is investigated. In order to see the symmetry properties clearly, the diagonal elements T_{nn}, the elements T_{mn} below the diagonal, $m > n$ ("conversion of the channel up"), and the elements T_{mn} above the diagonal, $m < n$ ("conversion of the channel down"), of the 3×3 matrix T are plotted separately.

The transmission matrix for an electron with $E_F = 15.8E_1$ in the left-turned bend with $R_0 = 0.5w$, $\Theta = \pi/2$ in magnetic fields is shown in Fig. 5. (The plots for the right-turned bend can be easily obtained by the reversal of the magnetic field.) There is no symmetry according to the reversal of the magnetic field for any of the elements T_{mn}. The only symmetry relation appearing in this case is $T_{mn}(B) = T_{nm}(B)$. In the left-turned bend, the interchannel scattering is extremely strong in the region of positive magnetic fields $0 \leq B \leq 20B_0$. The conversion between quantum channels in the bent wire can be controlled by the magnetic field. As seen from the plot and from the geometrical configuration, the mixing of channels is stronger when the electron is pushed by the Lorentz force to the inner wall with the larger curvature $1/R_0$. The interchannel scattering is weaker when the electron is guided by the Lorentz force along the outer wall with the smaller cur-

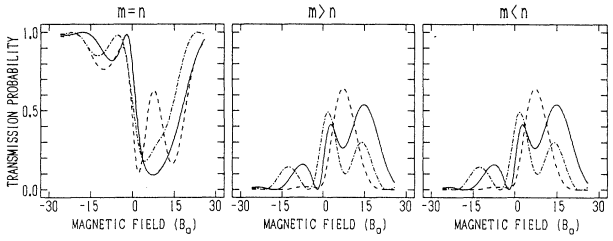

FIG. 5. The T matrix of the left-turned bend. The interchannel transmission probabilities T_{mn} are plotted as a function of the magnetic field (in units of B_0) for $E_F = 15.8E_1$, $R_0 = 0.5w$, and $\Theta = \pi/2$. Indication of plots: the diagonal elements T_{mn} ($m = n$) are in the left-side plot, the elements T_{mn} below the diagonal ($m > n$) are in the central plot, and the elements T_{mn} above the diagonal ($m < n$) are in the right-side plot. Line convention: T_{11}, T_{21}, T_{12}, solid curves; T_{22}, T_{31}, T_{13}, dashed curves; T_{33}, T_{32}, T_{23}, dash-dotted curves.

vature $1/(R_0+w)$. Since the backscattering is very small, the conductance [Eq. (2.7)] remains quantized and almost of the same value as in the perfect lead. The coupling of channels seems to weaken for the very strong magnetic fields $|B| \geq 25B_0$ when the magnetic length $l_B \leq w/5$ is very short. Because of $l_B < w$ and $l_B < R_0$ in such strong magnetic fields, the magnetic length becomes the most important length scale in the system, more important than w (the scale of the quantization of the transverse motion) or R_0 (the scale of the bending effects). In very strong magnetic fields, the transport in smooth bends enters the global adiabatic regime,[36] where the intermode transitions are absent in the whole system.

Next, we turn our attention to the transmission matrix of the S-shaped system composed of the left-turned bend, the straight wire of length L, and the right-turned bend. The geometrical parameters of the bends are $R_0=0.5w$ and $\Theta=\pi/2$. The Fermi energy of an electron is $E_F=15.8E_1$. The plots of the elements of the T matrix as a function of the magnetic field are shown in Fig. 6. The symmetry of the T matrix according to the transposition accompanied by the reversal of the magnetic field is apparent, $T_{mn}(-B)=T_{nm}(B)$. The conversion of channels

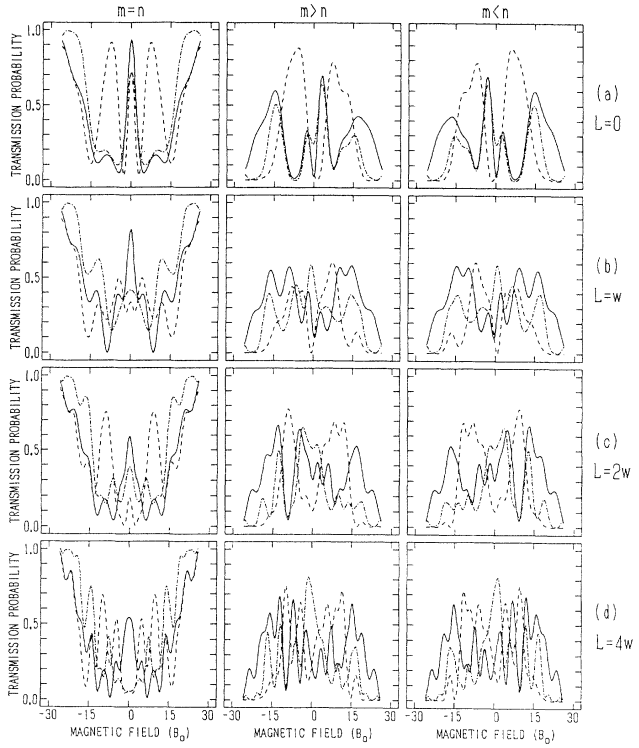

FIG. 6. The T matrix of the S-shaped system. The interchannel transmission probabilities T_{mn} are plotted as a function of the magnetic field (in units of B_0) for $E_F=15.8E_1$, $R_0=0.5w$, and $\Theta=\pi/2$. The distance between bends is (a) $L=0$, (b) $L=w$, (c) $L=2w$, and (d) $L=4w$. Indication of plots: the diagonal elements T_{mn} $(m=n)$ are in the left-side column, the elements T_{mn} below the diagonal $(m>n)$ are in the central column, and the elements T_{mn} above the diagonal $(m<n)$ are in the right-side column. The line convention is the same as in Fig. 5.

occurs strongly in the weak and moderate magnetic fields. In very strong magnetic fields, the mixing of channels seems to weaken as the magnetic length becomes very short, $l_B \ll R_0$. The region of the weak $(l_B \gg R_0)$ and moderate $(l_B \approx R_0)$ magnetic fields is filled with many oscillations in the T matrix. The increasing distance L between bends increases the number of oscillations. The period of the oscillations varies from the irregular case for $L=0$ to the nearly regular case for $L=4.0w$. These oscillations reveal the complicated structure of the multichannel interference of electrons restricted by the circular and straight hard-wall boundaries in the presence of magnetic fields. The magnetic-field dependence of the strength of the interchannel $(m \neq n)$ coupling can be evaluated by the construction of the envelope function to these oscillations. The oscillations of the interchannel scattering probabilities are distributed below an L-independent envelope function. The envelope function has its maximum in $B=0$ and decreases with the increasing absolute value of the magnetic field. The backscattering is not of any importance here. The conductance (in units of $2e^2/h$) remains almost equal to the number of open channels in the asymptotic regions.

The last system presented here in order to show the dependence of the elements of the T matrix on the magnetic field is the U-shaped quantum wire made of left-turned bends separated by the straight wire of length L. The geometrical parameters and the Fermi energy are the same as in the previous case. The plot of the elements of the T matrix is shown in Fig. 7. Similar to the single-bend case, the T matrix is symmetrical, $T_{mn}(B)=T_{nm}(B)$. The reversal of the magnetic field yields results for the U-shaped system made of the right-turned bends. The conversion of channels has no symmetry in reversed magnetic fields. The construction of the envelope function for $m \neq n$ shows that the interchannel scattering probabilities reach their maximum in the region of positive magnetic fields on the order of $10B_0$. The amplitude and the number of the quasiperiodic oscillations are dependent on the distance L. The backscattering is nearly absent and the conductance is almost equal to that of the ideal lead, as can be expected for this choice of parameters R_0, Θ, and E_F.

We have mentioned several times the symmetry of the T matrix of the single bend, the S-shaped system, and the U-shaped system. We can understand the symmetries of the S matrix not only in our special systems, but rather generally in the ballistic transport through two-terminal two-dimensional systems in the presence of magnetic fields. The important step is the use of the reciprocity[35] of the S matrix which can be stated in our case as

$$\tilde{t}_{mn}(B)=t_{nm}(-B) \ . \tag{3.1}$$

Only the reciprocity relation holds in any system regardless of the symmetry of the potential. If the confining potential has some geometrical symmetry, this symmetry will be reflected in some additional symmetry of the S matrix.

Let us consider a two-terminal system with the mirror-plane symmetry. The terminals are in different half-planes separated by the axis of the symmetry. The

Cartesian system of coordinates (x,y) can be found in which the relation for the potential, $V(x,y)=V(x,-y)$, holds. This is the case in the U-shaped system. Performing the mirror-plane reflection together with the inversion of the magnetic field yields an additional symmetry relation for the transmission amplitudes:

$$\tilde{t}_{mn}(B)=t_{mn}(-B) . \tag{3.2}$$

Combining this additional symmetry with the reciprocity relation results in the transpositional symmetry

$$t_{mn}(B)=t_{nm}(B) . \tag{3.3}$$

Next, let us consider a two-terminal system with the rotational symmetry $V(x,y)=V(-x,-y)$ (rotation of angle π, for example our S-shaped system). Leaving the magnetic field unchanged and performing only the rotation of angle π yield an additional symmetry relation for the transmission amplitudes:

$$\tilde{t}_{mn}(B)=(-1)^{m+n}t_{mn}(B) . \tag{3.4}$$

The factor $(-1)^{m+n}$ can be understood in the following way. Imagine, for example, the y coordinate as the transverse coordinate in the asymptotic regions. The change

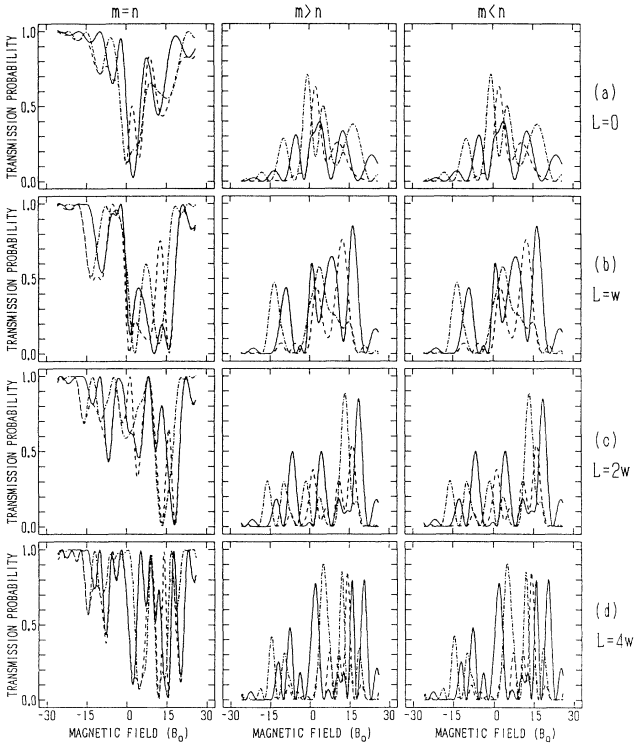

FIG. 7. The T matrix of the U-shaped system. The interchannel transmission probabilities T_{mn} are plotted as a function of the magnetic field (in units of B_0) for $E_F=15.8E_1$, $R_0=0.5w$, and $\Theta=\pi/2$. The distance between bends is (a) $L=0$, (b) $L=w$, (c) $L=2w$, and (d) $L=4w$. Indication of plots: the diagonal elements T_{mn} $(m=n)$ are in the left-side column, the elements T_{mn} below the diagonal $(m>n)$ are in the central column, and the elements T_{mn} above the diagonal $(m<n)$ are in the right-side column. The line convention is the same as in Fig. 5.

$y\rightarrow -y$ does not affect the transverse eigenfunctions with even symmetry; however, those with odd symmetry must be multiplied by (-1). Combination of this additional symmetry with the reciprocity relation gives

$$t_{mn}(B)=(-1)^{m+n}t_{nm}(-B) . \tag{3.5}$$

The reciprocity relation for the backscattering amplitudes is $r_{mn}(B)=r_{nm}(-B)$. The symmetry relations for the backscattering amplitudes are formally the same as Eqs. (3.2) or (3.4) for the transmission ones.

As was mentioned previously, an experimental approach which permits direct measurement of the entire T matrix of a mesoscopic conductor was reported.[34] One of the measurements was concerned with the modal features in the distribution function of electrons emerging from a quantum point contact (QPC). Although the conductance remained approximately quantized, Shepard, Roukes, and Van der Gaag[34] have found generation of higher modal components in the outgoing beam caused by the nonadiabatic widening of the potential in the exit zone of the QPC. The fact that the side lobes in the angular profile of electrons emerging from the QPC are asymmetric when the QPC is close to the pinch-off indicates that the proposed critical path may not be strictly symmetrical. The realistic model of the QPC must necessarily consider not only the transversely symmetric shape of the constriction but also the bendings and other asymmetries of the confining potential.[37] The scattering between even and odd modes is essentially present in systems with bends regardless of magnetic fields. The applied magnetic field, even a weak one of order B_0, can be used to control the intermode scattering probabilities.

We make one remark on the detection of electrons in individual channels. When the spin of electrons is not considered, the energies of individual channels are degenerated. However, when we take into account the spin-orbit interaction, which is sensitive to the shape of the orbital wave function, the degeneracy is lifted. The detection of electrons may then be enabled by the fine-structure splitting of the energies of individual channels. Unfortunately, the spin-orbit interaction in bend structures seems to be extremely small as was shown by Ikegami and Nagaoka[38] for the case of two-dimensional curved surfaces. We have done estimations[39] for bent quantum wires with similar results. The coupling constant Γ (in the dimensionless units of energy E_1) of the spin-orbit interaction is approximately $\Gamma\approx 10^{-6}w^{-2}$, where w is the width of the quantum wire in nm.

B. Backscattering and quasibound states

The backscattering is usually small in the system with circular bends. Nevertheless, the backscattering can appear for some choices of the geometrical parameters w, R_0, Θ, and the Fermi energy E_F. The smaller ratio of the inner radius R_0 to the width of the wire w gives the stronger backward scattering. In the single bend, the reflection occurs mainly for electrons at the beginning of each conductance plateau (see Fig. 1 in Ref. 31) and for electrons close to the end of each conductance plateau (see Fig. 4 in Ref. 32). In the double bends, separated by

distance about $L > w$, the increase of the conductance at the beginning of each plateau is not monotonic, but the conductance is modulated by shallow oscillations that disappear quickly with the increasing electron energies. These oscillations resemble resonances reported in the quantum wire with the inserted potential barrier[40] or with the constricted part of stepwise variation.[7]

The reflection that occurs in the vicinity of the end of each conductance plateau in the single circular bend is caused by the quasibound state. The quasibound state in the nth conductance plateau is formed by the wave function from the $(n+1)$th subband in the bend. The energy thresholds for propagation in the bend are slightly lower (see Table 1 in Ref. 33) than in the straight wire. Though the wave function from the $(n+1)$th subband can exist in the bend, it cannot propagate in the straight wire. Effectively, the influence of the bend is similar to the quantum well with a rather complicated potential profile dependent on the angular momentum [see the Appendix, Eq. (A3)].

We want to present the results for the reflection caused by the quasibound states for the S-shaped and the U-shaped systems in the absence and also in the presence of magnetic fields. First, we turn our attention to the vicinity of the end of the lowest conductance plateau in the absence of magnetic fields. The conductance as a function of the Fermi energy for various distances L between the bends is plotted in Fig. 8. When the distance L is short, $L \leq 2w$, only one quasibound state develops. For $L=0$, the energy of the quasibound state is about $3.99E_1$. The binding energy as a difference from the threshold energy of the second conductance plateau is then approximately $0.01E_1$. For $L=0$ and $L=0.25w$, the dip in the conductance of the S-shaped system is broader than the dip in the conductance of the U-shaped system. However, for $L=0.50w$ and $L=2.00w$, the S-shaped system shows a narrower dip than the U-shaped systems. For $L=1.00w$, the dips in both systems are of about the same width, although they differ in the energy by $\approx 0.004E_1$. When L becomes longer than about $2w$, another quasibound state with extremely small binding energy appears. Further increases of L gradually bring both quasibound states closer in energy. The nonmonotonic dependence of the binding energies of the quasibound states on the parameter L is noteworthy.[41] For the limit $L \to \infty$, we expect the degeneration in energy of both quasibound states. It follows from the symmetry considerations that the lower quasibound state must be of even symmetry and the higher one must be of odd symmetry. The odd-type quasibound state cannot be bound for $L \leq 2w$ (approximately), since for such short L its energy lies above the threshold energy for propagation in the second subband of the straight wire. The energy positions of the conductance dips are related to the binding energies of the quasibound states. The widths of the dips are related to the coupling of the quasibound state with the propagating modes in the straight leads. Both the energies and the widths of the dips show nonmonotonic dependence on the distance L. The conductance pattern is apparently different for the S-shaped and the U-shaped systems.

Next, the behavior of the conductance in the vicinity of the end of the lowest conductance plateau in the presence of magnetic fields is examined. The plot of the conductance for $B \neq 0$ is in Fig. 9. The development of one quasibound state for $L \leq 2w$ and of two quasibound states for $L \geq 2w$ is easy to recognize. Magnetic fields usually narrow the conductance dips, although this is not always true, as can be seen from the conductance of the S-shaped system for $L=2.00w$. In the U-shaped system, the dips become very shallow in several cases and may even disappear for $L=0.25w$. The dependence of binding energies on the distance L is changed to the almost monotonic one seen for S-shaped and U-shaped systems in $B=\pm 5B_0$. The sampling of the energy in Figs. 8 and 9 is done with the step $0.0001E_1$.

The further increases of magnetic fields narrow the width of conductance dips and shift their energy positions smoothly toward higher Fermi energies. The dips represent the coupling between extended states propagating in opposite directions in straight-wire regions (sub-

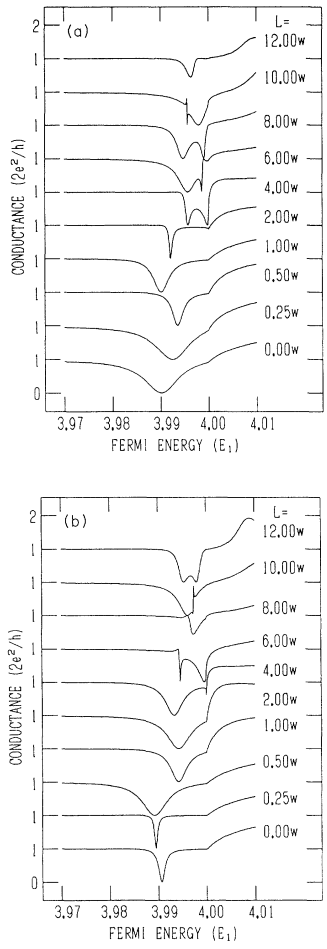

FIG. 8. The detailed structure of the antiresonances in the vicinity of the end of the lowest conductance plateau in the absence of magnetic fields. (a) The S-shaped system. (b) The U-shaped system. The zero-field conductance is plotted as a function of the Fermi energy for bends of $R_0=0.5w$ and $\Theta=\pi/2$ and for various distances L between bends.

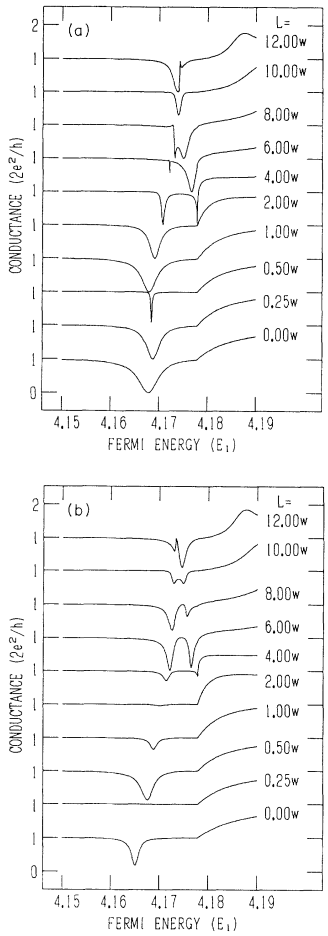

FIG. 9. The detailed structure of the antiresonances in the vicinity of the end of the lowest conductance plateau in the presence of magnetic fields. (a) The S-shaped system. (b) The U-shaped system. The conductance for $B=5B_0$ is plotted as a function of the Fermi energy for bends of $R_0=0.5w$ and $\Theta=\pi/2$ and for various distances L between bends.

band n) via localized orbits in bent-wire regions (subband $n+1$). The conductance dips or antiresonances correspond to the singularities (poles) of the S matrix in which the coupling reaches its maximum and the backscattering is the strongest. The singularities of the S matrix may be related to the conductance peaks or resonances if one considers a system with finite leads connected to widened parts instead of the system with infinite leads. In the system with finite leads, the bound state below the threshold energy of the lowest conductance plateau will also create the resonance.

IV. CONCLUSION

We have presented the exact quantum-mechanical formulation and the numerical solution of the multichannel ballistic magnetotransport in the two-dimensional quantum wires with double circular bends. The parameters of the investigated system can be expressed by the following length scales: the Fermi wavelength λ_F, the magnetic length l_B, the width of the wire w, the bending radius R_0, and the distance between bends L.

The transmission matrix has been evaluated for three propagating channels for various distances L between bends in the S-shaped and U-shaped systems. The interchannel scattering shows a rather complicated dependence on the magnetic field with many oscillations of variable period and amplitude, especially for longer L. The strong interchannel scattering is caused by the abrupt change of the effective potential for each subband at the interfaces between straight and bent wires. On these interfaces, either the longitudinal or the angular momentum is not integral of motion, as it is in the straight or bent wire, respectively. The elements of the T matrix in the two-terminal two-dimensional samples are restricted by the symmetry relation $T_{mn}(B)=T_{nm}(B)$ for the systems with the mirror-plane symmetry (each of terminals is in the different half-plane) or $T_{mn}(-B)=T_{nm}(B)$ for the systems with the rotational symmetry (rotation of angle π). The conductance may remain quantized in wide region of plateaus even in the presence of the interchannel scattering.[42] The interchannel scattering seems to weaken in strong magnetic fields when the system may reach the adiabatic transport regime.[36] However, in very strong magnetic fields, the electron-electron interactions become increasingly important and must be considered in detail.

The backscattering has been found at the beginning and the end of each conductance plateau. The coupling of the wave function from the higher subband in the bends to the wave function in the straight leads forms single or double conductance dips. The binding energies of related quasibound states are nonmonotonic functions of the distance between bends. The explanation of this dependence needs further investigation. The moderate magnetic field can also widen the conductance dips. Nevertheless, the dips become narrow and may gradually vanish in strong magnetic fields. This may be of particular interest in the application of quantum wires with bends.

Our method of calculation has been extended for the multiple-bend quantum wires with the periodic structure. We have found the formation of minibands and energy gaps in the conductance of finite periodic structures with repeated left-turned and right-turned bends.[43] The interchannel scattering in periodic structures in magnetic fields seems to be of eminent interest since the problem itself represents "skipping orbits" of electrons between periodically repeated circular surfaces.[44]

ACKNOWLEDGMENTS

The authors express their sincere thanks to S. Suga, H. Nakanishi, and M. Mizuno for useful discussions. One of us (K.V.) is indebted to H. U. Baranger, M. Büttiker, M. L. Roukes, and P. Středa for stimulating discussions. This work was supported in part by a Grant-in-Aid for Scientific Research on Priority Area, "Electron Wave Interference Effects in Mesoscopic Structures" from the Ministry of Education, Science, and Culture of Japan. The numerical calculations have been performed in the

Computation Center of The Osaka University on the supercomputer NEC SX-2N.

APPENDIX

Topics related to the properties of the solution to Eq. (2.13) are discussed here. We introduce a new function $h(r,\nu_l^{(\pm)})=g(r,\nu_l^{(\pm)})\sqrt{r}$. We eliminate the first derivative in Eq. (2.13) and obtain the eigenvalue equation

$$\left\{\frac{d^2}{dr^2}+\frac{1}{4r^2}+\frac{\pi^2}{w^2}\epsilon_F-\left[\frac{\nu_l^{(\pm)}}{r}+\frac{\mathcal{B}}{2w^2}r\right]^2\right\}h(r,\nu_l^{(\pm)})=0\ , \tag{A1}$$

with the boundary condition $h(r,\nu_l^{(\pm)})=0$ for $r=R_0$, R_0+w. Since the bend is an open system, the eigenvalues $\nu_l^{(\pm)}$ are not only integers, but they are real or complex numbers for propagating or evanescent channels, respectively. In the asymptotic limit $R_0\gg w$ the eigenvalues are approximately

$$\nu_l^{(\pm)}=-\frac{\mathcal{B}}{2}\left[\frac{R_0}{w}+\frac{1}{2}\right]^2 \pm\left[\left[\frac{R_0}{w}+\frac{1}{2}\right]^2\pi^2(\epsilon_F-l^2)+\frac{1}{4}\right]^{1/2}, \tag{A2}$$

which corresponds to the replacement of all possible paths of an electron in the bend by the path along the central radius r_c of the bend, $r_c=R_0+w/2$. In the general case of $R_0\approx w$, Eq. (A2) is used as an ansatz in the numerical solution. Equation (A1) is more suitable for the numerical solution and it also has clear physical meaning as it represents the one-dimensional Schrödinger equation with an effective potential

$$V_{\rm eff}(r)=\left[\frac{\nu_l^{(\pm)}}{r}+\frac{\mathcal{B}}{2w^2}r\right]^2-\frac{1}{4r^2}\ . \tag{A3}$$

In comparison with the potential in the straight wire, there are intervals of eigenvalues for which the effective potential is negative in the bend. This indicates the possibility of a bound or quasibound state. For example, in zero magnetic field, $V_{\rm eff}$ is always negative for an angular momentum $|L_z|\le\hbar/2$. In all channels, $l=1,2,\ldots,\infty$, there is a narrow band of energies in which an electron wave moves with the absolute value of angular momentum lower than $\hbar/2$. For the electron with angular momentum $|L_z|<\hbar/2$, the minimum of the effective potential is at the inner wall ($r=R_0$). For the electron moving with angular momentum $|L_z|>\hbar/2$, the minimum is at the outer wall ($r=R_0+w$).

The linear differential operator of the second order in Eqs. (2.13) and (A1) can be brought to the shape of the Sturm-Liouville (SL) operator.[45] The SL analysis of the orthogonality of the eigenfunctions gives

$$(\nu_m^{(\pm)}-\nu_n^{(\pm)})I(\nu_m^{(\pm)},\nu_n^{(\pm)})=(\nu_m^{(\pm)}-\nu_n^{(\pm)})\int_{R_0}^{R_0+w}dr\left[\frac{\nu_m^{(\pm)}+\nu_n^{(\pm)}}{r}+\frac{\mathcal{B}}{w^2}r\right]g(r,\nu_m^{(\pm)})g(r,\nu_n^{(\pm)})=0. \tag{A4}$$

We have chosen the normalization to the unit angular flux of electrons in each quantum channel, $|I(\nu_m^{(\pm)},\nu_n^{(\pm)})|=\delta(\nu_m^{(\pm)},\nu_n^{(\pm)})$. The canonical angular momentum $L_z=-i\hbar\partial/\partial\varphi$ of an electron in channel l is simply $\hbar\nu_l^{(\pm)}$. The operator of mechanical angular momentum, however, is $\mathcal{L}_z=-i\hbar\partial/\partial\varphi+eBr^2/2c$, where the dependence on radius r is a consequence of the magnetic flux penetration through the bent wire. The angular electron flux J_φ can be expressed through the operator of mechanical angular momentum $\mathcal{L}_z$,

$$J_\varphi=\frac{1}{2m^*}\int_{R_0}^{R_0+w}dr\left[\Psi^*(r,\varphi)\left[-\frac{i\hbar}{r}\frac{\partial}{\partial\varphi}+\frac{eBr}{2c}\right]\Psi(r,\varphi)+\Psi(r,\varphi)\left[\frac{i\hbar}{r}\frac{\partial}{\partial\varphi}+\frac{eBr}{2c}\right]\Psi^*(r,\varphi)\right]\ . \tag{A5}$$

By substitution of the mode expansion for the wave function, Eq. (2.12), into Eq. (A5) and by using the orthogonality relation (A4), we obtain the angular electron flux in the bend,

$$J_\varphi\propto\sum_{l=1}^{N}\{[c_l^{(+)}]^*c_l^{(+)}I(\nu_l^{(+)},\nu_l^{(+)})+[c_l^{(-)}]^*c_l^{(-)}I(\nu_l^{(-)},\nu_l^{(-)})\}\ , \tag{A6}$$

where the sum is over all electrons at the Fermi level, i.e., propagating channels. Taking $|I(\nu_l^{(+)},\nu_l^{(+)})|=|I(\nu_l^{(-)},\nu_l^{(-)})|=1$, we get the equal distribution of the angular flux of electrons into each propagating channel, as was wanted. This way of normalization saves us from the use of explicit angular velocity factors in the S matrix. The sign of the normalization constant I determines the orientation of the current in each channel. Since we associate the amplitudes $c_l^{(+)}$ with the motion in the positive direction of angle φ and the amplitudes $c_l^{(-)}$ with the motion in the negative direction of angle φ, we take $I(\nu_l^{(+)},\nu_l^{(+)})=+1$ and $I(\nu_l^{(-)},\nu_l^{(-)})=-1$ for propagating channels. The evanescent channels do not contribute directly to the net angular flux of electrons. However, they may penetrate with exponential decay (in the absence of magnetic fields) or with oscillatory exponential decay (in the presence of magnetic fields) through the barriers with the effective potential $V_{\rm eff}(r)$, and thus cause a tunneling current. Furthermore, the evanescent channels may form a bound state or quasibound state in the vicinity of the scattering region with the negative effective potential. The phase of the normalization constant I is determined from the symmetry $g(r,[\nu_l^{(\pm)}]^*,B)=[g(r,\nu_l^{(\pm)},B)]^*$ for the evanescent channels.

[1]For a review, see C. W. J. Beenakker and H. van Houten, in *Solid State Physics: Advances in Research and Applications,* edited by H. Ehrenreich and D. Turnbull (Academic, New York, 1991), Vol. 44, pp. 1–228.

[2]G. Timp, A. M. Chang, P. Mankiewich, R. Behringer, J. E. Cunningham, T. Y. Chang, and R. E. Howard, Phys. Rev. Lett. **59**, 732 (1987).

[3]M. L. Roukes, A. Scherer, S. J. Allen, Jr., H. G. Craighead, R. M. Ruthen, E. D. Beebe, and J. P. Harbison, Phys. Rev. Lett. **59**, 3011 (1987).

[4]C. J. B. Ford, S. Washburn, M. Büttiker, C. M. Knoedler, and J. M. Hong, Phys. Rev. Lett. **62**, 2724 (1989).

[5]G. Timp, H. U. Baranger, P. deVegvar, J. E. Cunningham, R. E. Howard, R. Behringer, and P. M. Mankiewich, Phys. Rev. Lett. **60**, 2081 (1988).

[6]L. P. Kouwenhoven, F. W. J. Hekking, B. J. van Wees, and C. J. P. M. Harmans, Phys. Rev. Lett. **65**, 361 (1990).

[7]H. Kasai, K. Mitsutake, and A. Okiji, J. Phys. Soc. Jpn. **60**, 1679 (1991).

[8]A. Okiji, H. Kasai, and K. Mitsutake, J. Phys. Soc. Jpn. **61**, 1717 (1992).

[9]A. Okiji, H. Kasai, and A. Nakamura, Prog. Theor. Phys. Suppl. **106**, 209 (1991).

[10]A. Okiji and H. Kasai, in *Transport Phenomena in Mesoscopic Systems,* edited by F. Fukuyama and T. Ando, Springer Series in Solid-State Sciences No. 109 (Springer-Verlag, Berlin, 1992), pp. 153–162.

[11]A. Nakamura, Y. Maki, and A. Okiji, J. Phys. Soc. Jpn. **60**, 749 (1991).

[12]A. Okiji, N. Negishi, and A. Nakamura, J. Phys. Soc. Jpn. **61**, 1145 (1992).

[13]For further review of the mode-matching method see, e.g., Refs. 16–19.

[14]T. Ando, Phys. Rev. B **44**, 8017 (1991).

[15]H. U. Baranger, D. P. DiVincenzo, R. A. Jalabert, and A. D. Stone, Phys. Rev. B **44**, 10 637 (1991).

[16]R. L. Schult, D. G. Ravenhall, and H. W. Wyld, Phys. Rev. B **39**, 5476 (1989).

[17]D. G. Ravenhall, H. W. Wyld, and R. L. Schult, Phys. Rev. Lett. **62**, 1780 (1989).

[18]Y. Avishai and Y. B. Band, Phys. Rev. Lett. **62**, 2527 (1989).

[19]R. L. Schult, H. W. Wyld, and D. G. Ravenhall, Phys. Rev. B **41**, 12 760 (1990).

[20]P. Exner, P. Šeba, and P. Št'ovíček, Czech. J. Phys. B **39**, 1181 (1989).

[21]A. Weisshaar, J. Lary, S. M. Goodnick, and V. K. Tripathi, Appl. Phys. Lett. **55**, 2114 (1989).

[22]J. Martorell, S. Klarsfeld, D. W. L. Sprung, and Hua Wu, Solid State Commun. **78**, 13 (1991).

[23]Hua Wu, D. W. L. Sprung, and J. Martorell, Phys. Rev. B **45**, 11 960 (1992).

[24]Y. Avishai, D. Bessis, B. G. Giraud, and G. Mantica, Phys. Rev. B **44**, 8028 (1991).

[25]Hua Wu, D. W. L. Sprung, and J. Martorell, J. Appl. Phys. **72**, 151 (1992).

[26]J. C. Wu, M. N. Wybourne, W. Yindeepol, A. Weisshaar, and S. M. Goodnick, Appl. Phys. Lett. **59**, 102 (1991).

[27]P. Exner and P. Šeba, J. Math. Phys. **30**, 2574 (1989).

[28]P. Exner and P. Šeba, Phys. Lett. A **144**, 347 (1990).

[29]D. W. L. Sprung, Hua Wu, and J. Martorell, J. Appl. Phys. **71**, 515 (1992).

[30]F. Sols and M. Macucci, Phys. Rev. B **41**, 11 887 (1990).

[31]C. S. Lent, Appl. Phys. Lett. **56**, 2554 (1990).

[32]K. Vacek, H. Kasai, and A. Okiji, J. Phys. Soc. Jpn. **61**, 27 (1992).

[33]K. Vacek, A. Okiji, and H. Kasai, Technol. Rep. Osaka Univ. **42**, 225 (1992).

[34]K. L. Shepard, M. L. Roukes, and B. P. Van der Gaag, Phys. Rev. Lett. **68**, 2660 (1992).

[35]M. Büttiker, IBM J. Res. Dev. **32**, 317 (1988).

[36]L. I. Glazman and M. Jonson, Phys. Rev. B **41**, 10 686 (1990).

[37]J. A. Nixon and J. H. Davies, Phys. Rev. B **41**, 7929 (1990); M. J. Laughton, J. R. Barker, J. A Nixon, and J. H. Davies, *ibid.* **44**, 1150 (1991).

[38]M. Ikegami and Y. Nagaoka (unpublished).

[39]K. Vacek, A. Okiji, and H. Kasai (unpublished).

[40]P. F. Bagwell, Phys. Rev. B **41**, 10 354 (1990); A. Kumar and P. F. Bagwell, *ibid.* **43**, 9012 (1991).

[41]For the broken-strip double-bend configuration with right angles, the binding energies of bound states below the first conductance plateau are shown in Ref. 23, and the binding energies are a monotonic function of the distance L.

[42]For some other mesoscopic systems, the quantization of conductance in the presence of the interchannel scattering can be found in Refs. 7 and 14 and in E. Castaño and G. Kirczenow, Phys. Rev. B **45**, 1514 (1992).

[43]K. Vacek, A. Okiji, and H. Kasai, Solid State Commun. (to be published).

[44]The classical two-dimensional skipping of electrons on the surfaces of convex semicircles is a stochastic problem; see G. M. Zaslavsky, Phys. Rep. **80**, 157 (1981).

[45]E. Butkov, *Mathematical Physics* (Addison-Wesley, New York, 1968), Sec. 9.3.